Frontiers of Physics
https://doi.org/10.1007/s11467-021-1083-8
Front. Phys.
16(5), 53505 (2021)

ERRATUM

Erratum to: Effect of biaxial strain and hydrostatic pressure on the magnetic properties of bilayer CrI_3

Chong Xu[1], Qian-Jun Wang[1], Bin Xu[1], Jun Hu[1,2,†]

[1] *School of Physical Science and Technology & Jiangsu Key Laboratory of Thin Films, Soochow University, Suzhou 215006, China*
[2] *School of Physical Science and Technology, Ningbo University, Ningbo 315211, China*
Corresponding author. E-mail: [†]hujun2@nbu.edu.cn
Received May 14, 2021; accepted May 18, 2021

ERRATUM TO: *Front. Phys.* 53502 (2021), https://doi.org/10.1007/s11467-021-1073-x

The latest version of the original publication of this article is attached. The online version of the original article can be found at https://doi.org/10.1007/s11467-021-1073-x and http://journal.hep.com.cn/fop/EN/10.1007/s11467-021-1073-x.

*This article can also be found at http://journal.hep.com.cn/fop/EN/10.1007/s11467-021-1083-8.

Frontiers of Physics
https://doi.org/10.1007/s11467-021-1073-x
Front. Phys.
16(5), 53502 (2021)

RESEARCH ARTICLE

Effect of biaxial strain and hydrostatic pressure on the magnetic properties of bilayer CrI_3

Chong Xu[1], Qian-Jun Wang[1], Bin Xu[1], Jun Hu[1,2,†]

[1] *School of Physical Science and Technology & Jiangsu Key Laboratory of Thin Films, Soochow University, Suzhou 215006, China*
[2] *School of Physical Science and Technology, Ningbo University, Ningbo 315211, China*
Corresponding author. E-mail: †hujun2@nbu.edu.cn
Received January 19, 2021; accepted April 8, 2021

Two-dimensional van der Waals magnetic materials are intriguing for applications in the future spintronics devices, so it is crucial to explore strategy to control the magnetic properties. Here, we carried out first-principles calculations and Monte Carlo simulations to investigate the effect of biaxial strain and hydrostatic pressure on the magnetic properties of the bilayer CrI_3. We found that the magnetic anisotropy, intralayer and interlayer exchange interactions, and Curie temperature can be tuned by biaxial strain and hydrostatic pressure. Large compressive biaxial strain may induce a ferromagnetic-to-antiferromagnetic transition in both CrI_3 layers. The hydrostatic pressure could enhance the intralayer exchange interaction significantly and hence largely boost the Curie temperature. The effect of the biaxial strain and hydrostatic pressure revealed in the bilayer CrI_3 may be generalized to other two-dimensional magnetic materials.

Keywords bilayer CrI_3, biaxial strain, hydrostatic pressure, magnetic properties

1 Introduction

Van der Waals two-dimensional (2D) materials have evoked great interest of researchers in the community of condensed matter physics and materials science, since the discovery of graphene [1], because they exhibit abundant new physical properties, and are promising in various applications in electronic and optoelectronic devices [2]. Recently, a new class of 2D materials — 2D ferromagnetic (FM) materials — have been discovered [3, 4]. The 2D FM materials are particularly interesting not only in the aspect of fundamental science, because it was unexpected according to the Mermin–Wagner theorem [5], but also in the development of new generation of spintronics devices, because the highest Curie temperature (T_C) may even achieve to room temperature [6–9].

The bulk CrI_3 is FM with the T_C of 61 K and a rhombohedral layer stacking [10, 11]. The FM ordering persists in few-layer CrI_3 except bilayer, with the T_C down to 45 K for the monolayer CrI_3, whereas the bilayer CrI_3 displays interlayer antiferromagnetic (AFM) coupling [4]. It is known that the physical properties may be closely associated with the stacking order in 2D matertials [12]. Indeed, a series of literatures have reported that the interlayer magnetic coupling in the bilayer CrI_3 depends on the stacking pattern [13–16]. With the AB-stacking order [Fig. 1(a)] where the top layer laterally shifts by $[\frac{2}{3}, \frac{1}{3}]$ in fractional coordinates with respect to the bottom layer, the two CrI_3 layers couple ferromagnetically. With the AB′-stacking order [Fig. 1(b)] where the lateral shift is $[\frac{1}{3}, \frac{1}{3}]$, the two CrI_3 layers couple antiferromagnetically. In fact, these two types of stacking orders correspond to the bulk CrI_3 at low temperature (below 210 K) with the space group $R\bar{3}$ and room temperature with the space group $C2/m$, respectively [11, 17]. Nevertheless, the AB′-stacking bilayer CrI_3 was usually observed in experiment, probably because the bilayer exfoliated at room temperature is kinetically trapped in the AB′-stacking order during the cooling process [13]. Interestingly, the interlayer magnetism of the bilayer CrI_3 can be tuned by electric field, gate voltage and external pressure [17–21].

Magnetic anisotropy (MA) is an important requirement for realizing long-range magnetic ordering in 2D magnetic materials [4, 22], because the long-range 2D magnetic ordering cannot establish in the spin-rotational invariant systems as demonstrated in the Mermin–Wagner theorem [5]. Magnetic anisotropy plays the role of breaking the spin rotational invariance, and thus allows the long-range 2D magnetic ordering to exist. For the sake of practical applications in spintronics devices, perpendicular magnetic anisotropy (PMA) and FM ordering at

*arXiv: 2104.13525. This article can also be found at http://journal.hep.com.cn/fop/EN/10.1007/s11467-021-1073-x.

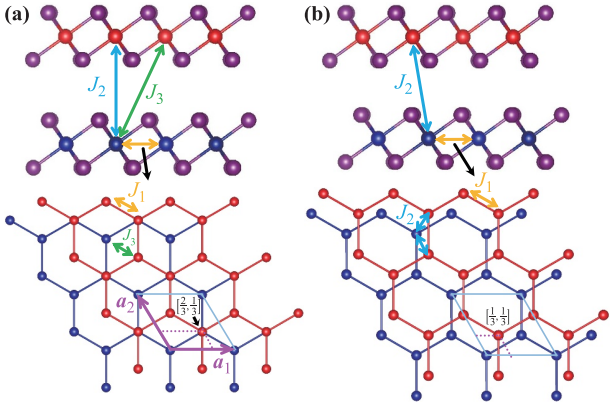

Fig. 1 Side and top views of the atomic structure of bilayer CrI_3 with **(a)** AB-stacking order and **(b)** AB′-stacking order. The red and blue spheres stand for the Cr atoms in the top and bottom layers, respectively. The purple spheres stand for the I atoms. The intralayer (J_1) and interlayer (J_2 and J_3) exchange parameters are indicated. In the bottom layers, only the Cr atoms are shown, and the light blue parallelograms denote the unit cells of the AB- and AB′-stacking bilayers. The purple arrows mark the lattice vectors, and the purple dotted lines indicate the lateral shift (in fractional coordinates) of the top layer (red) with respect to the bottom layer.

room temperature are required simultaneously. Therefore, strong PMA and FM ordering are desired and it is important to explore strategies to control the MA and to enhance T_C [23]. Although theoretical study of the effect of strain on the MA of the monolayer CrI_3 has been done recently [24–27], systematic theoretical investigation of the electronic and magnetic properties including the MA and magnetic ordering of the bilayer CrI_3 under strain is still lacking [28].

In this paper, we explored the effect of biaxial strain and hydrostatic pressure on the electronic and magnetic properties of the bilayer CrI_3, based on first-principles calculations and Monto Carlo simulation. We found that the magnetic properties of the bilayer CrI_3 are sensitive to biaxial strain and hydrostatic pressure. In particular, the hydrostatic pressure may turn the easy axis from the out-of-plane direction (i.e., PMA) to in-plane direction. The intralayer exchange interaction may be significantly enhanced by the hydrostatic pressure, which may lead to T_C over 100 K, much higher than the original T_C without the hydrostatic pressure.

2 Computational details

The atomic structures, electronic and magnetic properties were calculated by using the Vienna *ab-initio* simulation package in the framework of the density functional theory (DFT) [29, 30]. The interaction between valence electrons and ionic cores was described within the framework of the projector augmented wave (PAW) method [31, 32]. Van der Waals interaction was included with the optB86b exchange functional [33, 34]. Hubbard U of 3 eV for the Cr atom was adopted to account for the strong electronic correlations [35]. The energy cutoff for the plane wave basis expansion was set to 650 eV. The two-dimensional Brillouin zone was sampled by a 24×24 k-grid mesh. The atomic positions were fully relaxed using the conjugated gradient method until the force on each atom is smaller than 0.01 eV/Å.

The exchange coupling parameters of the bilayer CrI_3 can be extracted by comparing the total energies with different spin configurations (see Fig. 2), based on the Heisenberg spin Hamiltonian

$$H = -\sum_{i,j} J_{ij} \boldsymbol{S}_i \cdot \boldsymbol{S}_j. \quad (1)$$

As illustrated in Fig. 1, we considered the first nearest neighboring intralayer exchange interaction (denoted by J_1) for both AB- and AB′-stacking bilayers. For the interlayer couplings, the dominant exchange interactions can be represented by J_2 and J_3 for the AB-stacking bilayer CrI_3 [Fig. 1(a)] and J_2 for the AB′-stacking bilayer CrI_3 [Fig. 1(b)]. With these exchange interaction parameters, we performed Monte Carlo simulations with a 64×64 supercell to estimate the T_C.

3 Results and discussion

We started our calculations from the experimental lattice constant of the bulk CrI_3 ($a_0 = 6.867$ Å), and then applied in-plane biaxial strain (ε) from –6% to 6%. The negative and positive signs indicate compressive and extensile strains, respectively. The corresponding lattice constant varies from 6.45 Å to 7.28 Å. Accordingly, the distance between the nearest Cr atoms increases from 3.73 Å to 4.20 Å, and the Cr–I bond lengths increase from 2.71 Å to 2.79 Å, as plotted in Fig. 3(a). Clearly, the variation of the Cr–I bond lengths (from –1.45% and 1.45%) is much smaller than the in-plane biaxial strain, because the out-of-plane positions of the Cr and I atoms are free to relax. Consequently, the Cr–I–Cr angle (α) increases significantly when the strain varies from –6% to 6%, as shown in Fig. 3(b). There are two types of I–Cr–I angles, the angle formed by one Cr atom and two I atoms lying in the same atomic plane (two atomic planes) is denoted as θ_1 (θ_2). θ_1 increases but slower than α, while θ_2 decreases significantly, as seen in Fig. 3(b). Note that these structural parameters do not depend on the stacking patterns.

The bilayer CrI_3 is semiconducting with the band gap of 1.01 and 1.07 eV, respectively for the AB- and AB′-stacking bilayers, slightly smaller than that of the monolayer CrI_3 (1.09 eV). Generally speaking, the band gap of a semiconductor will increase (decrease) under compressive (extensile) strain, as sketched in Fig. 4(a). However, the band gap of the bilayer CrI_3 exhibits opposite trend. As shown in Figs. 4(c) and (d), the band gaps of

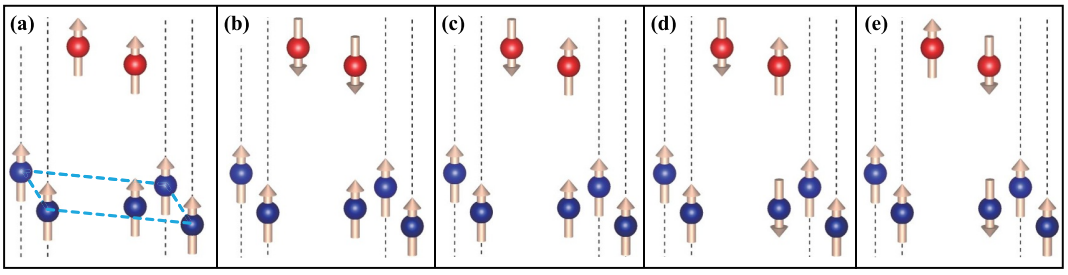

Fig. 2 Magnetic configurations of AB-stacking bilayer CrI_3. The dashed parallelogram denotes the in-plane unit cell. **(a)** Intralayer and interlayer ferromagnetism. **(b)** Intralayer ferromagnetism and interlayer antiferromagnetism. **(c)** Interlayer ferrimagnetism. The bottom CrI_3 layer is ferromagnetic, while the top CrI_3 layer is antiferromagnetic. **(d)** Intralayer and interlayer antiferromagnetism. **(e)** Intralayer antiferromagnetism and interlayer ferromagnetism. The magnetic configurations of AB′-stacking bilayer CrI_3 are similar.

the AB- and AB′-stacking bilayers respectively decrease to 0.74 and 0.69 eV under compressive strain of –6%, while they increase to 1.13 and 1.22 eV under extensile strain of 6%. This abnormal phenomenon can be explained by the feature of the local structure which is represented by the distorted octahedron formed by one Cr atom and six I atoms as displayed in Fig. 4(b). In the local coordinate frame, the 3d orbitals of the Cr atom split into the triplet t_{2g} orbital and the doublet e_g orbital due to the crystal field, as seen from the inset in Fig. 4(c). The band gap lies between the occupied t_{2g} states and the empty e_g states, and thus is primarily determined by the crystal-field splitting. When a compressive (extensile) biaxial strain is applied onto the unit cell, the equivalent strain onto the octahedron is actually extensile (compressive) along the C_3 axis as indicated in Fig. 4(b). Therefore, the compressive (extensile) biaxial strain leads to the octahedron to be stretched (compressed), and thus weakens (strengthens) the crystal-field splitting. Consequently, the energy levels of the e_g states decrease (increase), resulting in the decrease (increase) of the band gap. Clearly, the evolution of the band gap under external strain still accords with the trend shown in Fig. 4(a), if we consider the equivalent strain on the octahedron rather than the biaxial strain on the unit cell.

The biaxial strain also tunes the magnetic properties. As shown in Fig. 5, the local spin moment contributed by the Cr atoms ($M_{S,Cr}$) increases as the strain change from –6% to 6%. In other words, the larger lattice constant results in the larger $M_{S,Cr}$. The total increment of $M_{S,Cr}$ is about 0.1 μ_B. However, the total spin moment of each CrI_3 formula is independent of the strain and maintains 3.0 μ_B. It is clear that the value of $M_{S,Cr}$ is larger than the total spin moment, because the I atoms contribute about –0.1 μ_B per atom. Note that the stacking patterns do not

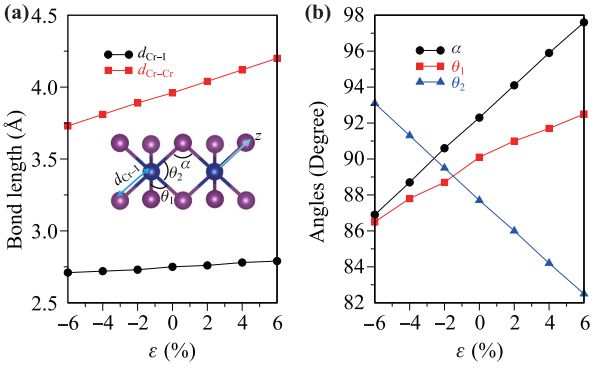

Fig. 3 Structure parameters of the AB-stacking bilayer CrI_3 under biaxial strain. **(a)** The Cr–I bond length (d_{Cr-I}) and the distance between the nearest Cr atoms (d_{Cr-Cr}). **(b)** Two types of the I–Cr–I angles and Cr–I–Cr angle. The z axis of the local coordinate frame is indicated.

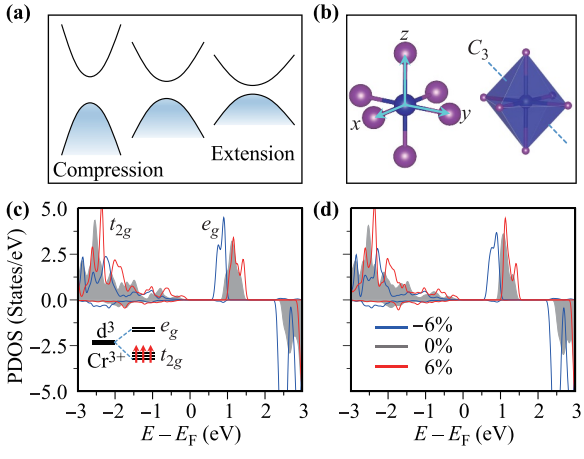

Fig. 4 **(a)** Sketch of the conventional evolution of the band structure under biaxial strain. **(b)** One CrI_6 octahedron with the local coordinate frame. The dashed line indicates the C_3 rotational axis and it is the direction of the equivalent strain on the octahedron to the biaxial strain on the unit cell. **(c, d)** Projected density of states (PDOS) of the 3d orbital of the Cr^{3+} ion under biaxial strains for the AB- and AB′-stacking bilayers, respectively. Positive (negative) sign refers to spin majority (minority) channel. The inset in (c) shows the schematic energy splitting of the 3d orbitals of the Cr^{3+} ion.

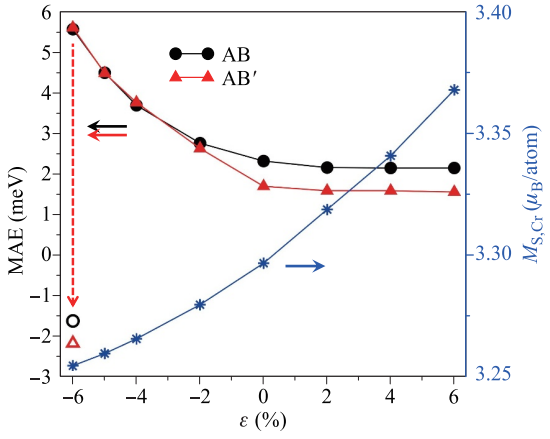

Fig. 5 Magnetic anisotropy energy (MAE) and local magnetic spin moment on Cr atom ($M_{S,Cr}$) of the AB-stacking bilayer CrI_3 under biaxial strain. The dashed arrow indicates the change of MAE when the FM-to-AFM transition occurs.

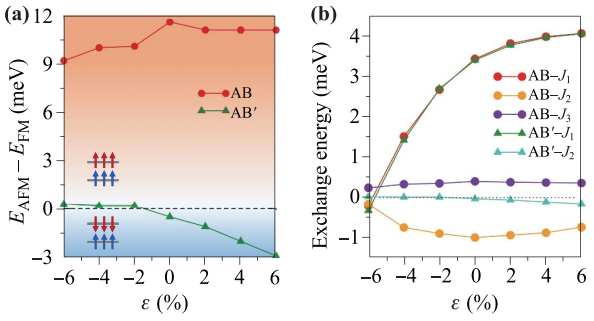

Fig. 6 **(a)** Energy difference between the interlayer FM and AFM states of the bilayer CrI_3 under biaxial strain. **(b)** Exchange interaction energies between the Cr atoms as indicated in Fig. 1.

affect the spin moments. The magnetic anisotropy energy (MAE) are positive for all strains, indicating PMA for the bilayer CrI_3, in agreement with experimental observations [4]. In addition, the MAE increases significantly when the amplitude of the compressive strain increases, while it decreases slightly when the extensile strain increases, similar with a recent report [26]. Furthermore, the MAE of the AB-stacking bilayer CrI_3 is larger than that of the AB′-stacking bilayer CrI_3 in most range of the strains. At the experimental lattice constant (i.e., $\varepsilon = 0$), the MAEs of the AB- and AB′-stacking bilayers are 0.58 meV and 0.34 meV per CrI_3 formula, respectively, in agreement with the recent report [23]. When $\varepsilon = -6\%$, the MAE becomes 1.4 meV per CrI_3 formula for both AB- and AB′-stacking bilayers. Obviously, larger MAE guarantees better thermal stability at high temperature.

Note that the properties discussed above do not depend on the interlayer exchange interaction. The two CrI_3 layers may couple with each other either ferromagnetically or antiferromagnetically [4]. The ground state can be determined by calculating the energy difference between the FM and AFM states: $\Delta E = E_{AFM} - E_{FM}$. As shown in Fig. 6(a), the AB-stacking bilayer CrI_3 manifests strong interlayer ferromagnetism for the whole range of the strain. On the contrary, a FM-to-AFM transition occurs near $\varepsilon = -2\%$ for the AB′-stacking bilayer CrI_3. With compressive strain $\varepsilon \leq -2\%$, the two CrI_3 layers couple with each other ferromagnetically with the magnetic configuration in Fig. 2(a). The interlayer coupling becomes AFM for minor compressive strain and all extensile strain, and the corresponding magnetic configuration is similar with that plotted in Fig. 2(b). Therefore, the ground state of the AB′-stacking bilayer CrI_3 is interlayer AFM, in agreement with the experimental observation [4].

To reveal the underlying mechanism of the exchange couplings under the biaxial strain, we calculated the total energies of five different magnetic configurations as plotted in Fig. 2. In the framework of Heisenberg model given by Eq. (1), the total energies related to the exchange couplings for the five different magnetic configurations in Fig. 2 for the AB-stacking bilayer CrI_3 can be written as follows: $E_a = -(6J_1 + J_2 + 9J_3)S^2$; $E_b = -(6J_1 - J_2 - 9J_3)S^2$; $E_c = -(J_2 - 3J_3)S^2$; $E_d = +(6J_1 + J_2 - 3J_3)S^2$; $E_e = +(6J_1 - J_2 + 3J_3)S^2$. For the AB′-stacking bilayer CrI_3, the total energies are $E_a^{'} = -(6J_1 - 4J_2)S^2$; $E_b^{'} = -(6J_1 + 4J_2)S^2$; $E_c^{'} = 0$; $E_d^{'} = +6J_1S^2$; $E_e^{'} = +6J_1S^2$. Here, $S = 3/2$ is the spin quantum number of each CrI_3 formula. Then we can obtain these exchange interaction parameters.

Figure 6(b) plots the exchange interaction parameters. It can be seen that the intralayer exchange interaction energy (J_1) increases when the extensile strain increases and decreases when the compressive strain increases, for both AB- and AB′-stacking bilayers. The amplitudes of J_1 of the AB- and AB′-stacking bilayers are almost the same. In other words, the intralayer exchange interaction in bilayer CrI_3 depends on the lattice constant monotonically but is independent of the stacking patterns. The larger lattice constant results in the larger J_1. In addition, the sign of J_1 changes around $\varepsilon = -6\%$, which indicates a intralayer FM-to-AFM transition. Similar magnetic phase transition was also observed in the monolayer CrI_3 [26, 27]. With the extensile strain ($\varepsilon > 0$) and moderate compressive strain ($-6\% < \varepsilon < 0$), the neighboring Cr atoms in the same CrI_3 layer couple with each other ferromagnetically. Combined the FM and AFM interlayer couplings respectively for the AB- and AB′-stacking bilayers, the AB- and AB′-stacking bilayers adopt the magnetic configurations displayed in Figs. 2(a) and (b), respectively, in this situation. With large compressive strain ($\varepsilon \leq -6\%$), the intralayer exchange interaction becomes AFM. Since the interlayer coupling is FM for both AB- and AB′-stacking bilayers, they adopt the magnetic configuration shown in Fig. 2(e). This magnetic configuration is the same as that reported recently [28]. The trend of the strain-dependent exchange interactions can be understood qualitatively as

follows. It has been revealed that J_1 contains two parts of contributions: the direct exchange interaction between the first nearest neighboring Cr atom via t_{2g}–t_{2g} orbitals and the indirect superexchange interaction via the t_{2g}–p–e_g orbitals [23–27]. Because of the octahedral crystal-field splitting, the former favors AFM exchange interaction, while the later favors FM exchange interaction. With extensive strain and moderate compressive strain, the indirect superexchange interaction dominates the intralayer exchange interaction in the CrI_3 layer, which results in the FM ground state and positive J_1. Furthermore, when the lattice constant increases, the Cr–Cr distance and the Cr–I–Cr angle (α in Fig. 3) increases. Consequently, the direct exchange interaction is weakened, while the superexchange interaction is enhanced due to the stronger t_{2g}–p hybridization. These combined effects make J_1 increases. With large compressive strain $\varepsilon \leq -6\%$, the Cr–Cr distance is short enough, so that the Cr–Cr direct exchange interaction dominates, resulting in AFM ground state and negative J_1. Moreover, when $\varepsilon = -6\%$, the MAEs of the AB- and AB′-stacking bilayers are –1.60 and –2.15 meV, respectively, as indicated by open symbols in Fig. 5, implying in-plane MA rather than PMA.

For the interlayer exchange interactions of the AB-stacking bilayer CrI_3, J_2 is negative and its amplitudes in the most range of the strain are large, indicating that the two Cr atoms connected by J_2 (see Fig. 1) prefer AFM coupling. J_3 is positive and its amplitude is smaller than that of J_2. For each Cr atom, there is only one pair of exchange interaction represented by J_2, while there are six pairs of exchange interaction represented by J_3. Therefore, the final interlayer exchange interaction is FM. For the AB′-stacking bilayer CrI_3, the amplitudes of J_2 are relatively small, and the sign changes around $\varepsilon = -2\%$, corresponding to the FM-to-AFM transition as shown in Fig. 6(a).

With the exchange interaction parameters, we carried out Monte Carlo (MC) simulation based on the Heisenberg model as expressed in Eq. (1). Although the bulk CrI_3 is believed to be Ising type FM magnet [4], we found that the Ising model overestimates T_C greatly. For the monolayer CrI_3, the Curie temperatures from the Ising model, Heisenberg model, and mean-field theory are 130 K, 90 K and 52 K, respectively. Apparently, only the mean-field theory predicts proper T_C close to the experiment measurement (45 K). Nevertheless, the mean-field theory could not be applied to the bilayer CrI_3 due to the complicated exchange interactions. Therefore, we choose the Heisenberg model to estimate the Curie temperatures of the bilayer CrI_3 under biaxial strains. Although the amplitudes of the Curie temperatures are expected to be overestimated, qualitative investigation of the response of T_C to the biaxial strain is still meaningful.

Figure 7(a) plots the magnetization (i.e., the average spin moment per CrI_3 formula) as a function of temperature for the AB′-stacking bilayer CrI_3, from the MC simulations. It can be seen that the average spin moment sharply decreases from $3\mu_B$ to 0 at certain temperature for each strain, corresponding to the T_C. The Curie temperatures of the strain-free AB- and AB′-stacking bilayers increase to about 130 K and 100 K (i.e., at $\varepsilon = 0$), respectively, which means that both the interlayer FM exchange interaction in the AB-stacking bilayer CrI_3 and the interlayer AFM exchange interaction in the AB′-stacking bilayer CrI_3 have positive effect on the FM ordering, compared to the monolayer CrI_3. With the strain varing from –6% to 6%, the T_C increases from 11 K to 160 K for the AB-stacking bilayer CrI_3 and from 9 K to 130 K for the AB′-stacking bilayer CrI_3, as shown in Fig. 7(b). This trend is similar to that of J_1, indicating that the T_C is mainly determined by the intralayer exchange interactions in the bilayer CrI_3, similar to the monolayer CrI_3. The FM ordering in the AB-stacking bilayer CrI_3 is further enhanced by the interlayer exchange interactions, which leads to higher T_C with respect to the AB′-stacking bilayer CrI_3 at the same strain. It is worth noting that the stability of the magnetic ordering depends on not only the T_C but also the MAE. Although the MAEs of the bilayer CrI_3 under extensile biaxial strain decrease slightly relative to strain-free case (see Fig. 5), the MAEs are already large enough to ensure the magnetic ordering bellow Curie temperatures for both AB- and AB′-stacking bilayers.

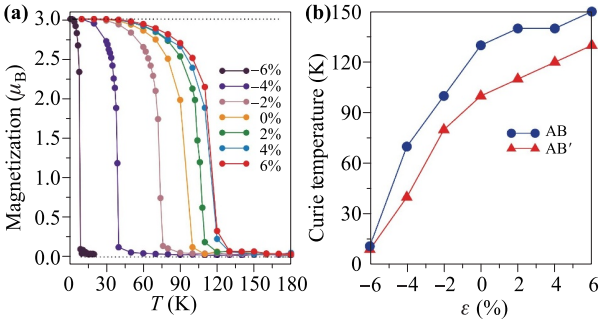

Fig. 7 **(a)** Magnetization (average spin moment per CrI_3 formula) of the AB′-stacking bilayer CrI_3 at different temperatures. **(b)** Curie temperature of the bilayer CrI_3 under biaxial strain.

Expect for the biaxial strain, the hydrostatic pressure may also modify the magnetism of the bilayer CrI_3 [20, 21]. Because the interlayer distance is much easier to be changed than the lateral lattice constant, the hydrostatic pressure can be regarded as the compressive strain on the octahedron along the C_3 axis as denoted in Fig. 4(b). Here, we use the decrement of the distance between the two CrI_3 layers (Δd) to represent the hydrostatic pressure. We firstly calculated the energy difference between the interlayer FM and AFM states, as plotted in Fig. 8(a). For the AB-stacking bilayer CrI_3, ΔE keeps positive and increases rapidly as Δd increases, which indicates that the interlayer exchange is strongly FM. This can also be manifested by the rapidly increasing J_2 and positive J_3

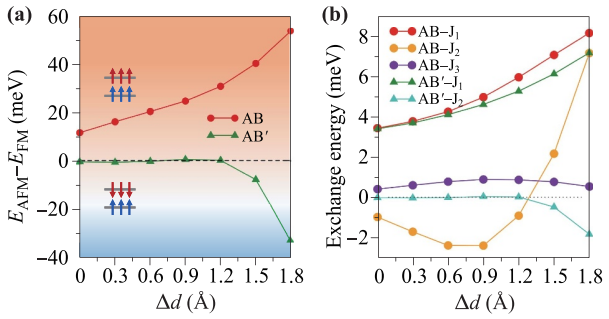

Fig. 8 **(a)** Energy difference between the interlayer FM and AFM states of the bilayer CrI_3 under hydrostatic pressure. **(b)** Exchange interaction energies between the Cr atoms as indicated in Fig. 1.

as shown in Fig. 8(b). For the AB′-stacking bilayer CrI_3, ΔE increases slightly first, then decreases strikingly when $\Delta d > 1.2$ Å. In addition, the sign of ΔE at $\Delta d = 0.9$ and 1.2 Å is positive, implying that the AB′-stacking bilayer CrI_3 favors the interlayer AFM state at this situation.

The intralayer exchange interactions in both AB- and AB′-stacking bilayers remain FM, as manifested by the positive values of J_1 in Fig. 8(b). Moreover, J_1 increases monotonically as Δd increases for both systems, and the magnitudes of J_1 are much larger than the others at the same biaxial strain. Therefore, the Curie temperatures increase significantly up to 320 K and 280 K respectively for the AB- and AB′-stacking bilayers, as shown in Fig. 9(a). Although T_C is overestimated by the Heisenberg model, the relative enlargement could be instructive. Considering that the amplitudes of T_C of the AB- and AB′-stacking bilayers have been enlarged by about 2.5 times at $\Delta d =$ 1.8 Å compared to those at pressure-free systems, T_C over 100 K could be expected in real experimental measurement.

The MAE of the AB-stacking bilayer CrI_3 decreases monotonically as Δd increases, as shown in Fig. 9(b). For the AB′-stacking bilayer CrI_3, the MAE decreases first, then increases at $\Delta d = 0.9$ Å, and decreases again when $\Delta d > 0.9$ Å. In fact, the AB′-stacking bilayer CrI_3 favors the interlayer FM state at $\Delta d = 0.9$ and 1.2 Å as seen in Fig. 8(a), so that the MAEs behave differently from the other points. If the AB′-stacking bilayer CrI_3 is in the interlayer AFM state, the MAEs follow the trend formed by the other points, as manifested by the open triangles and connected by the blue dashed lines in Fig. 9(b). When $\Delta d > 1.5$ Å, the MAEs of both AB- and AB′-stacking bilayers are negative, indicating in-plane MA. Nonetheless, the amplitudes of the MAEs are comparable to or even larger than those of the press-free systems, especially for $\Delta d = 1.8$ Å, hence the magnetic ordering could still be retained bellow T_C.

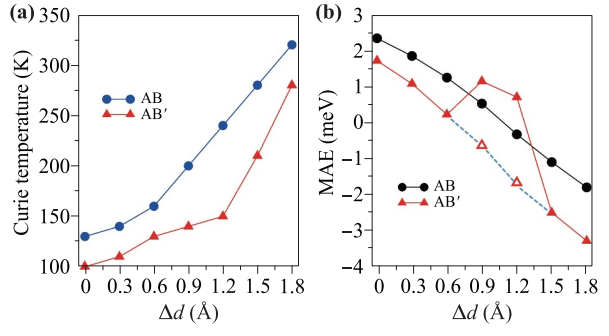

Fig. 9 **(a)** Curie temperature and **(b)** magnetic anisotropy energy (MAE) of the bilayer CrI_3 under hydrostatic pressure. The open triangles were calculated with interlayer AFM state for the AB′-stacking bilayer CrI_3.

4 Conclusions

In summary, we investigated the electronic and magnetic properties of two types of bilayer CrI_3 under biaxial strain and hydrostatic pressure, based on first-principles calculations and Monto Carlo simulation. We found that the band gaps, MAEs, intralayer and interlayer exchange interactions, and Curie temperatures can be tuned by the biaxial strain and hydrostatic pressure. The band gap decreases (increases) under compressive (extensile) strain, which is related to the symmetry of the CrI_6 octahedron. The MAE increases under compressive strain, but decreases under extensile strain and hydrostatic pressure. The interlayer FM coupling of the AB-stacking bilayer CrI_3 is robust under both biaxial strain and hydrostatic pressure. The interlayer coupling of the AB′-stacking bilayer CrI_3 is sensitive to the biaxial strain. It prefers the interlayer AFM state under extensile strain and small compressive strain ($\varepsilon > -2\%$), but turns to the interlayer FM state for larger compressive stain. For both bilayers, the intralayer magnetic ordering may undergo a FM-to-AFM transition under large compressive strain ($\varepsilon < -6\%$). The interlayer exchange interaction may be significantly enhanced by the hydrostatic pressure, which may boost the Curie temperature over 100 K.

Acknowledgements This work was supported by the National Natural Science Foundation of China (No. 11574223) and the Six Talent Peaks Project of Jiangsu Province (No. 2019-XCL-081).

References

1. 1. K. S. Novoselov, A. K. Geim, S. V. Morozov, D. Jiang, Y. Zhang, S. V. Dubonos, I. V. Grigorieva, and A. A. Firsov, Electric field effect in atomically thin carbon films, *Science* 306(5696), 666 (2004)
2. X. M. Li, L. Tao, Z. F. Chen, H. Fang, X. S. Li, X. R. Wang, J. B. Xu, and H. W. Zhu, Graphene and related two-dimensional materials: Structure-property relation-

ships for electronics and optoelectronics, *Appl. Phys. Rev.* 4(2), 021306 (2017)

3. C. Gong, L. Li, Z. Li, H. Ji, A. Stern, Y. Xia, T. Cao, W. Bao, C. Wang, Y. Wang, Z. Q. Qiu, R. J. Cava, S. G. Louie, J. Xia, and X. Zhang, Discovery of intrinsic ferromagnetism in two-dimensional van der Waals crystals, *Nature* 546(7657), 265 (2017)
4. B. Huang, G. Clark, E. Navarro-Moratalla, D. R. Klein, R. Cheng, K. L. Seyler, D. Zhong, E. Schmidgall, M. A. McGuire, D. H. Cobden, W. Yao, D. Xiao, P. Jarillo-Herrero, and X. D. Xu, Layer-dependent ferromagnetism in a van der Waals crystal down to the monolayer limit, *Nature* 546(7657), 270 (2017)
5. N. D. Mermin and H. Wagner, Absence of ferromagnetism or anti-ferromagnetism in one- or two-dimensional isotropic Heisenberg models, *Phys. Rev. Lett.* 17(22), 1133 (1966)
6. M. Bonilla, S. Kolekar, Y. Ma, H. C. Diaz, V. Kalappattil, R. Das, T. Eggers, H. R. Gutierrez, M. H. Phan, and M. Batzill, Strong room-temperature ferromagnetism in VSe_2 monolayers on van der Waals substrates, *Nat. Nanotechnol.* 13(4), 289 (2018)
7. Y. Deng, Y. Yu, Y. Song, J. Zhang, N. Z. Wang, Z. Sun, Y. Yi, Y. Z. Wu, S. Wu, J. Zhu, J. Wang, X. H. Chen, and Y. B. Zhang, Gate-tunable room-temperature ferromagnetism in two-dimensional Fe_3GeTe_2, *Nature* 563(7729), 94 (2018)
8. C. Gong and X. Zhang, Two-dimensional magnetic crystals and emergent heterostructure devices, *Science* 363(6428), eaav4450 (2019)
9. B. Huang, M. A. McGuire, A. F. May, D. Xiao, P. Jarillo-Herrero, and X. D. Xu, Emergent phenomena and proximity effects in two-dimensional magnets and heterostructures, *Nat. Mater.* 19(12), 1276 (2020)
10. J. F. Jr Dillon and C. E. Olson, Magnetization, resonance, and optical properties of the ferromagnet CrI_3, *J. Appl. Phys.* 36(3), 1259 (1965)
11. M. A. McGuire, H. Dixit, V. R. Cooper, and B. C. Sales, Coupling of crystal structure and magnetism in the layered, ferromagnetic insulator CrI_3, *Chem. Mater.* 27(2), 612 (2015)
12. T. Latychevskaia, S. K. Son, Y. Yang, D. Chancellor, M. Brown, S. Ozdemir, I. Madan, G. Berruto, F. Carbone, A. Mishchenko, and K. S. Novoselov, Stacking transition in rhombohedral graphite, *Front. Phys.* 14, 13608 (2019)
13. N. Sivadas, S. Okamoto, X. D. Xu, C. J. Fennie, and D. Xiao, Stacking-dependent magnetism in bilayer CrI_3, *Nano Lett.* 18(12), 7658 (2018)
14. P. H. Jiang, C. Wang, D. C. Chen, Z. C. Zhong, Z. Yuan, Z. Y. Lu, and W. Ji, Stacking tunable interlayer magnetism in bilayer CrI_3, *Phys. Rev. B* 99(14), 144401 (2019)
15. D. Soriano, C. Cardoso, and J. Fernández-Rossier, Interplay between interlayer exchange and stacking in CrI_3 bilayers, *Solid State Commun.* 299, 113662 (2019)
16. S. W. Jang, M. Y. Jeong, H. Yoon, S. Ryee, and M. J. Han, Microscopic understanding of magnetic interactions in bilayer CrI_3, *Phys. Rev. Mater.* 3(3), 031001 (2019)
17. S. Jiang, J. Shan, and K. F. Mak, Electric-field switching of two-dimensional van der Waals magnets, *Nat. Mater.* 17(5), 406 (2018)
18. B. Huang, G. Clark, D. R. Klein, D. MacNeill, E. Navarro-Moratalla, K. L. Seyler, N. Wilson, M. A. McGuire, D. H. Cobden, D. Xiao, W. Yao, P. Jarillo-Herrero, and X. D. Xu, Electrical control of 2D magnetism in bilayer CrI_3, *Nat. Nanotechnol.* 13(7), 544 (2018)
19. X. X. Zhang, L. Li, D. Weber, J. Goldberger, K. F. Mak, and J. Shan, Gate-tunable spin waves in antiferromagnetic atomic bilayers, *Nat. Mater.* 19(8), 838 (2020)
20. T. Li, S. Jiang, N. Sivadas, Z. Wang, Y. Xu, D. Weber, J. E. Goldberger, K. Watanabe, T. Taniguchi, C. J. Fennie, K. Fai Mak, and J. Shan, Pressure-controlled interlayer magnetism in atomically thin CrI_3, *Nat. Mater.* 18(12), 1303 (2019)
21. T. C. Song, Z. Y. Fei, M. Yankowitz, Z. Lin, Q. N. Jiang, K. Hwangbo, Q. Zhang, B. S. Sun, T. Taniguchi, K. Watanabe, M. A. McGuire, D. Graf, T. Cao, J. H. Chu, D. H. Cobden, C. R. Dean, D. Xiao, and X. D. Xu, Switching 2D magnetic states via pressure tuning of layer stacking, *Nat. Mater.* 18(12), 1298 (2019)
22. J. L. Lado and J. Fernández-Rossier, On the origin of magnetic anisotropy in two dimensional CrI_3, *2D Mater.* 4, 035002 (2017)
23. F. Xue, Y. Hou, Z. Wang, and R. Wu, Two-dimensional ferromagnetic van der Waals $CrCl_3$ monolayer with enhanced anisotropy and Curie temperature, *Phys. Rev. B* 100(22), 224429 (2019)
24. J. Liu, P. Mo, M. Shi, D. Gao, and J. Lu, Multiscale analysis of strain-dependent magnetocrystalline anisotropy and strain-induced Villari and Nagaoka-Honda effects in a two-dimensional ferromagnetic chromium tri-iodide monolayer, *J. Appl. Phys.* 124(4), 044303 (2018)
25. J. Liu, M. Shi, J. Lu, and M. P. Anantram, Analysis of electrical-field-dependent Dzyaloshinskii-Moriya interaction and magnetocrystalline anisotropy in a two-dimensional ferromagnetic monolayer, *Phys. Rev. B* 97(5), 054416 (2018)
26. L. Webster and J. A. Yan, Strain-tunable magnetic anisotropy in monolayer $CrCl_3$, $CrBr_3$, and CrI_3, *Phys. Rev. B* 98(14), 144411 (2018)
27. F. Zheng, J. Zhao, Z. Liu, M. Li, M. Zhou, S. Zhang, and P. Zhang, Tunable spin states in the two-dimensional magnet CrI_3, *Nanoscale* 10(29), 14298 (2018)
28. A. M. León, J. W. González, J. Mejía-López, F. Crasto de Lima, and E. S. Morell, Strain-induced phase transition in CrI_3 bilayers, *2D Mater.* 7, 035008 (2020)
29. G. Kresse and J. Furthmüller, Efficiency of ab-initio total energy calculations for metals and semiconductors using a plane-wave basis set, *Comput. Mater. Sci.* 6(1), 15 (1996)
30. G. Kresse and J. Furthmüller, Efficient iterative schemes for ab initio total-energy calculations using a plane-wave basis set, *Phys. Rev. B* 54(16), 11169 (1996)
31. P. E. Blöchl, Projector augmented-wave method, *Phys. Rev. B* 50(24), 17953 (1994)

32. G. Kresse and D. Joubert, From ultrasoft pseudopotentials to the projector augmented-wave method, *Phys. Rev. B* 59(3), 1758 (1999)
33. J. P. Perdew, K. Burke, and M. Ernzerhof, Generalized gradient approximation made simple, *Phys. Rev. Lett.* 77(18), 3865 (1996)
34. J. Klimeš, D. R. Bowler, and A. Michaelides, Van der Waals density functionals applied to solids, *Phys. Rev. B* 83(19), 195131 (2011)
35. A. I. Liechtenstein, V. I. Anisimov, and J. Zaanen, Density-functional theory and strong interactions: Orbital ordering in Mott–Hubbard insulators, *Phys. Rev. B* 52(8), R5467 (1995)